Toward ultimate miniaturization of high Q silicon traveling-wave microresonators

Mohammad Soltani, Qing Li, Siva Yegnanarayanan, and Ali Adibi*

School of Electrical and Computer Engineering, Georgia Institute of Technology, 777 Atlantic Drive NW, Atlanta, GA 30332-0250, USA

**adibi@ece.gatech.edu*

Abstract: High Q traveling-wave resonators (TWR)s are one of the key building block components for VLSI Photonics and photonic integrated circuits (PIC). However, dense VLSI integration requires small footprint resonators. While photonic crystal resonators have shown the record in simultaneous high Q (~10^5-10^6) and very small mode volumes; the structural simplicity of TWRs has motivated many ongoing researches on miniaturization of these resonators with maintaining Q in the same range. In this paper, we investigate the scaling issues of silicon traveling-wave microresonators down to ultimate miniaturization levels in SOI platforms. Two main constraints that are considered during this down scaling are: 1) Preservation of the intrinsic Q of the resonator at high values, and 2) Compatibility of resonator with passive (active) integration by preserving the SiO_2 BOX layer (plus a thin Si slab layer for P-N junction fabrication). Microdisk and microdonut (an intermediate design between disk and ring shape) are considered for high Q, miniaturization, and single-mode operation over a wide wavelength range (as high as the free-spectral range). Theoretical and experimental results for miniaturized resonators are demonstrated and Q's as high as ~10^5 for resonators as small as 1.5 μm radius are achieved.

OCIS codes: (130.3120) Integrated optics devices; (230.5750) Resonators

References and links

1. M. Lipson, "Silicon photonics: An exercise in self control," Nat. Photonics **1**(1), 18–19 (2007).
2. C. Gunn, "CMOS Photonics for High-Speed Interconnects," IEEE Micro **26**(2), 58–66 (2006).
3. Q. Xu, B. Schmidt, S. Pradhan, and M. Lipson, "Micrometre-scale silicon electro-optic modulator," Nature **435**(7040), 325–327 (2005).
4. J. Ahn, M. Fiorentino, R. Beausoleil, N. Binkert, A. Davis, D. Fattal, N. Jouppi, M. McLaren, C. Santori, R. Schreiber, S. Spillane, D. Vantrease, and Q. Xu, "Devices and architectures for photonic chip-scale integration," Appl. Phys., A Mater. Sci. Process. **95**(4), 989–997 (2009).
5. M. S. Nawrocka, T. Liu, X. Wang, and R. R. Panepucci, "Tunable silicon microring resonator with wide free special range," Appl. Phys. Lett. **89**(7), 071110 (2006).
6. Q. Xu, D. Fattal, and R. G. Beausoleil, "Silicon microring resonators with 1.5-μm radius," Opt. Express **16**(6), 4309–4315 (2008).
7. S. Xiao, M. H. Khan, H. Shen, and M. Qi, "A highly compact third-order silicon microring add-drop filter with a very large free spectral range, a flat passband and a low delay dispersion," Opt. Express **15**(22), 14765–14771 (2007).
8. M. R. Watts, D. C. Trotter, R. W. Young, and A. L. Lentine, Ultra-low power silicon microdisk modulators and switches," IEEE Conf. Group IV Photonics, Sorento, Italy, 2008.
9. S. Manipatruni, L. Chen, K. Preston, and M. Lipson, "Ultra-low power electro-optic modulator on silicon: towards direct logic driven silicon modulators," *Conference on Lasers and Electro-Optics* (CLEO), San Jose, CA, 2010.
10. M. Soltani, Q. Li, S. Yegnanarayanan, and A. Adibi, "Ultimate miniaturization of single and coupled resonator filters in silicon photonics," Conference on Laser and Electro-optics (CLEO), Baltimore, MD, 2009.
11. J. Shainline, S. Elston, Z. Liu, G. Fernandes, R. Zia, and J. Xu, "Subwavelength silicon microcavities," Opt. Express **17**(25), 23323–23331 (2009).

#130161 - $15.00 USD Received 14 Jun 2010; revised 18 Aug 2010; accepted 24 Aug 2010; published 30 Aug 2010

12. A. M. Prabhu, A. Tsay, Z. Han, and V. Van, "Ultracompact SOI microring add-drop filter with wide bandwidth and wide FSR," IEEE Photon. Technol. Lett. **21**(10), 651–653 (2009).
13. K. Srinivasan, M. Borselli, O. Painter, A. Stintz, and S. Krishna, "Cavity *Q*, mode volume, and lasing threshold in small diameter AlGaAs microdisks with embedded quantum dots," Opt. Express **14**(3), 1094–1105 (2006).
14. M. Soltani, Q. Li, S. Yegnanrayanan, B. Momeni, A. A. Eftekhar, and A. Adibi, "Large-scale array of small high-*Q* microdisk resonators for on-chip spectral analysis," IEEE LEOS Conference, Turkey, 2009.
15. F. Xia, M. Rooks, L. Sekaric, and Y. Vlasov, "Ultra-compact high order ring resonator filters using submicron silicon photonic wires for on-chip optical interconnects," Opt. Express **15**(19), 11934–11941 (2007).
16. M. Soltani, S. Yegnanarayanan, and A. Adibi, "Ultra-high *Q* planar silicon microdisk resonators for chip-scale silicon photonics," Opt. Express **15**(8), 4694–4704 (2007).
17. M. Borselli, T. Johnson, and O. Painter, "Beyond the Rayleigh scattering limit in high-*Q* silicon microdisks: theory and experiment," Opt. Express **13**(5), 1515–1530 (2005).
18. C. P. Michael, M. Borselli, T. J. Johnson, C. Chrystal, and O. Painter, "An optical fiber-taper probe for wafer-scale microphotonic device characterization," Opt. Express **15**(8), 4745–4752 (2007).
19. M. Soltani, Q. Li, S. Yegnanarayanan, and A. Adibi, "Improvement of thermal properties of ultra-high *Q* silicon microdisk resonators," Opt. Express **15**(25), 17305–17312 (2007).
20. T. J. Johnson, M. Borselli, and O. Painter, "Self-induced optical modulation of the transmission through a high-*Q* silicon microdisk resonator," Opt. Express **14**(2), 817–831 (2006).
21. M. Soltani, *Novel integrated silicon nanophotonic structures using ultra-high Q resonator*, Ph.D. dissertation, Georgia Institute of Technology, 2009.
22. F. L. Teixeira, and W. C. Chew, "Systematic derivation of anisotropic PML absorbing media in cylindrical and spherical coordinates," IEEE Microwave Guided Wave Lett. **7**(11), 371–373 (1997).
23. M. Soltani, S. Yegnanarayanan, Q. Li, and A. Adibi, "Systematic engineering of waveguide-resonator coupling for silicon microring/microdisk/racetrack resonators: theory and experiment," IEEE J. Quantum Electron. **46**(8), 1158–1169 (2010).
24. W. M. Green, M. J. Rooks, L. Sekaric, and Y. A. Vlasov, "Ultra-compact, low RF power, 10 Gb/s silicon Mach-Zehnder modulator," Opt. Express **15**(25), 17106–17113 (2007).
25. M. Borselli, *High-Q microresonators as lasing elements for silicon photonics*, Ph.D dissertation, California Institute of Technology, 2006.
26. C. Manolatou, M. J. Khan, S. Fan, P. R. Villeneuve, H. A. Haus, and J. D. Joannopoulos, "Coupling of modes analysis of resonant channel add-drop filtering," J. Lightwave Technol. **35**, 1322 (1999).
27. A. H. Atabaki, A. A. Eftekhar, S. Yegnanarayanan, and A. Adibi, "Novel micro-heater structure for low-power and fast photonic reconfiguration," *Conference on Lasers and Electro-Optics* (CLEO), San Jose, CA, 2010.

1. Introduction

Optical traveling-wave resonator (TWR) structures have been extensively employed for the realization of many on-chip photonic devices [1–4]. One of the major research directions, in such devices, has been the miniaturization of resonator sizes, especially in the silicon-on-insulator (SOI) platform [5–12]. This is because of the potential of SOI for monolithic electronic-photonic integration. In an SOI platform, the high refractive index contrast between the silicon and the oxide (BOX) layer enables shrinking the size of the resonators while preserving a high quality factor (*Q*). The rationale for resonator down-scaling is manifold. The obvious advantage is a smaller footprint for resonator-based devices. Correspondingly, large scale integration of functionalized high *Q* resonators is envisioned [4]. Additionally, free-spectral range (FSR) scales inversely proportional to the resonator size and the increased FSR can be highly advantageous for high-throughput wavelength-division multiplexing (WDM) systems [4] and spectroscopic applications [14]. Also, for resonator-based modulators and switches, small resonators are preferred as their power consumptions is directly proportional to the size of the resonator [8,9]. The TWR miniaturization has also been pursued in III-V materials (while preserving a very high *Q*) for enhancing light-matter interaction and cavity quantum electrodynamics (QED) effects and the results have been very promising [13].

In some of the previous studies, in an SOI platform, small silicon microring resonators with radii ranging from 1.5 μm-2.0 μm have been investigated [5–7]. The typical experimental *Q*'s reported for such miniaturized Si microrings fall within the range of 5,000-15,000 [5,6]. For these small microrings, the intrinsic *Q* of the resonator (i.e., Q_i which is the *Q* when the resonator is isolated and not coupled to a waveguide or any other devices) is limited by the radiation loss because of the sharp bend as well as the scattering loss because of the sidewall

#130161 - $15.00 USD Received 14 Jun 2010; revised 18 Aug 2010; accepted 24 Aug 2010; published 30 Aug 2010

roughness, and the trend of Q at very small radii is eventually governed by the radiation loss (or correspondingly radiation Q (Q_{rad})), predominantly. Racetrack resonators, as an extension of microring structures, have been a promising architecture for providing a stronger waveguide-resonator coupling and they have been extensively used for many functionalities [15]. However, achieving very compact sizes and large *FSR*s with this resonator architecture (while preserving a high Q_i) is challenging. This is mainly due to the presence of a large modal mismatch between the straight portion and the bend portion of the racetrack resonator, especially for the small bend radii and as a result the resonator loss dramatically increases [6]. Hence, racetrack resonators may not be the best choice when high Q_i and very small size (large *FSR*) resonators are simultaneously needed. For the sake of miniaturization, microdisk resonators are more promising compared to microring and racetrack. This is because of perfect circular symmetry and presence of one sidewall which forms a whispering gallery mode (WGM) at the perimeter of the microdisk [see Fig. 1(a) and 1(b)]. Such microdisk resonators can have a very high Q_i [16,17]. In contrast to microdisks, microring resonators have two sidewalls [see Fig. 1(a) and 1(c)]. A closer examination reveals that the inner sidewall of microrings will force the mode energy distribution out of the resonator as the bend radius is reduced, resulting in more energy leakage into the radiation modes. Also, the exposure of optical field to this additional sidewall will increase the scattering loss, further degrading the Q_i. Thus, it is naturally expected that microdisk resonators will exhibit higher Q_i than microrings under similar conditions of size and radius.

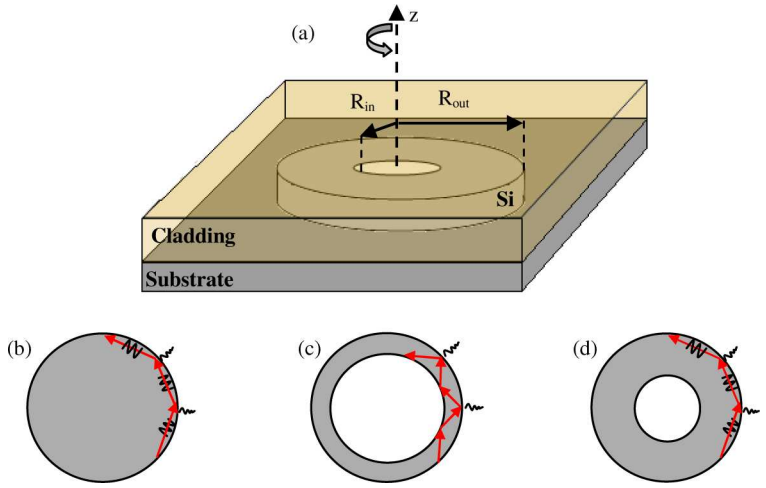

Fig. 1. (a) Structure of an axially symmetric silicon TWR structure seated on a substrate and covered by a cladding material. When R_{in} is zero the resonator is a microdisk; otherwise it is a microring or a microdonut. A ray approaches to the propagation of the traveling mode of the resonator for (b) a microdisk, (c) a microring, and (d) a microdonut. The mode leakage from the external wall of the resonators due to sidewall bending is shown.

The presence of the multiple radial modes can make the microdisk resonators inappropriate for applications that require a single resonance operation over the entire or a large portion of the *FSR*. In contrast, microring resonators do not exhibit such multiple radial modes for small ring widths. This issue of multiple radial mode operation of a conventional microdisk can be alleviated by modifying the conventional microdisk architecture to that of a microring with a thicker ring width [18]. In this device architecture, which can also be termed as a microdonut resonator [see Fig. 1(a) and 1(d)], the donut width is optimized in such a way that the internal wall of the donut has minimal interactions with the first radial mode of the resonator and very strong interactions with the higher order modes, thereby rendering these higher-order modes strongly radiative. We will show that such microdonut resonator architecture is promising for realizing miniaturized and high Q resonators.

#130161 - $15.00 USD Received 14 Jun 2010; revised 18 Aug 2010; accepted 24 Aug 2010; published 30 Aug 2010

In this paper, we investigate the scaling of silicon traveling-wave microresonators down to ultimate miniaturization levels in an SOI platform. Two main constraints that are considered during this down scaling are: (1) preservation of the intrinsic Q of the resonator at high values (e.g. $Q_i \sim 10^5$) and (2) compatibility of resonator with active or passive integration. Microdisk and microdonut resonators are introduced as the promising architectures for achieving such ultimate miniaturization and high Q, and their performances are compared. A constraint in the design is to preserve the oxide (BOX) layer (i.e. no undercutting). This BOX layer is found to be necessary both for thermal management [19] and ease of dense integration with other electronic and photonic devices. Resonators with both air and oxide cladding are considered during the size scaling analysis. In addition, miniaturized resonator architectures in which the resonator is seated on a thin silicon slab, suitable for electronic integration [3] is also studied. Single mode operation over the entire *FSR* range is achieved in optimized scaled microresonators without incurring significant radiation losses. Experimental results for miniaturized resonators with radii ranging from 1.5μm to 2.5μm are provided and compared with the theoretical simulation results.

The organization of the paper is as follows: Section 2 discusses the theoretical modeling and optimization of the resonator and impact of the resonator scaling on the Q and electromagnetic mode volume of the resonator. Section 3 provides the experimental results and the necessary discussions. Finally, conclusions are made in Section 4.

2. High Q and Miniaturized TWR: Design and optimization

In practice, the Q of a Si resonator is related to the aggregate of its intrinsic radiation loss (i.e. bending loss), when the resonator is ideal, and the losses resulted from other non-idealities introduced by fabrication imperfections and linear and nonlinear absorption properties of Si. The total Q (Q_t) of a resonator coupled to a waveguide can be expressed as

$$Q_t^{-1} = Q_{linear}^{-1} + Q_{nonlinear}^{-1} = [Q_{rad}^{-1} + Q_{b,abs}^{-1} + Q_{s,abs}^{-1} + Q_{scat}^{-1} + Q_c^{-1}] + [Q_{TPA}^{-1} + Q_{TPA-FC}^{-1}] \quad (1)$$

where, Q_{linear} is the contribution of linear losses to the total Q. Q_{linear} is composed of intrinsic radiation Q (Q_{rad}), the material bulk absorption Q ($Q_{b,abs}$), the surface state absorption Q ($Q_{s,abs}$ which is the absorption loss in the resonator due to generation of free carriers via surface electronic states at resonator surfaces), the Rayleigh scattering Q (Q_{scat}, which quantifies the coupling of the resonator mode to the radiation mode due to the surface roughness) [17], and the coupling Q (Q_c which quantifies the coupling of the resonator to the waveguide). The Q_i is the outcome of Q_{rad}, $Q_{b,abs}$, $Q_{s,abs}$, and Q_{scat}. $Q_{nonlinear}$ is the manifestation of nonlinearity-induced loss, which is composed of Q_{TPA} (which quantifies the loss of the resonator mode due to the two-photon absorption (TPA) at high optical powers) [20], and $Q_{TPA\text{-}FC}$ (which quantifies the resonator loss due to the TPA-induced free-carrier absorption) [20].

At lower powers in which the nonlinear contribution to the Q_i is negligible (and is the case of this paper), the total Q can be represented by the terms in the first bracket in Eq. (1). For an ideal resonator we are interested to find Q_{rad}, especially at miniaturized radii where Q_{rad} can be the dominant term in determining the Q_i of the resonator. In the following subsection, we theoretically model the resonator to extract its Q_{rad}.

2.1 Modeling the TWR and the Q_{rad}

We simulate TWRs with different radii using the finite-element method (FEM) in the vectorial form in cylindrical coordinates. A detailed discussion on the FEM implementation can be found in Ref [21]. The FEM formulation is based on the magnetic Helmholtz equation

#130161 - $15.00 USD Received 14 Jun 2010; revised 18 Aug 2010; accepted 24 Aug 2010; published 30 Aug 2010

$$\nabla \times [\frac{1}{n^2} \nabla \times \bar{H}] = (\frac{\omega_0}{c})^2 \bar{H} \quad (2)$$

where $\bar{H}$ represents the magnetic field vector; n is the refractive index; c is the speed of light; and ω_0 is the resonance frequency. ω_0 can be a complex number to contain the information about the resonator Q_{rad}. Because of the cylindrical symmetry of the structure, the magnetic field can be written as

$$\bar{H} = \bar{\mathrm{H}}(\rho, z) \exp(i\omega_0 t - im\varphi) \quad (3)$$

where m is the azimuthal harmonic mode number of the resonator; and ρ, z and ϕ represent the coordinates in the cylindrical system. The outer boundaries of the domain are terminated by axially-symmetric perfectly-matched layer (PML) absorbing boundary conditions [22]. Therefore, we are able to extract the real and imaginary part of the resonance frequency and from that to extract the intrinsic quality factor as

$$Q_{rad} = Real(w_0) \ / \ [2Imag(w_0)]. \quad (4)$$

The differential equation in Eq. (2) with the field axial symmetry given by Eq. (3) is reformulated to be implemented in the COMSOL Multiphysics to take the advantage of its mode solver and graphical user interface. In all the analysis shown in this paper, the thickness of the Si resonator is 230 nm (a thicker Si device layer can increase the radiation Q, however because of the commonly used thickness in the range of 200-250nm we have chosen this value of thickness). In the analysis, the refractive index of the silicon and oxide are 3.475 and 1.444, respectively; and the polarization of the resonator mode is TE (electric field predominantly in the plane of the resonator). The choice of TE is because it provides a higher Q_{rad} compared to the TM polarization (magnetic field predominantly in the plane of the resonator) at small radii. This is because the traveling mode of the resonator for the TM polarization has a lower effective index compared the one for the TE case. At smaller bending radii, a lower effective mode index result in a larger bending loss. In order to get a better understanding for this we can look at the effective index. The effective index of the traveling mode of a resonator is given by [23]

$$n_{eff} = \frac{\beta_\varphi}{(\omega_0 / c)} = \frac{2\pi m / (2\pi R)}{(\omega_0 / c)} = \frac{mc}{R\omega_0} \quad (5)$$

where β_ϕ is the azimuthal propagation constant of the traveling mode, c is speed of light, m is the azimuthal harmonic mode number mentioned in Eq. (3), and R is the resonator radius. When going to smaller radii, it can be shown that n_{eff} (or equivalently, the ratio m/R) becomes smaller. This can be qualitatively explained through the fact that at smaller bending radii mode energy extends more to the outside of the resonator which results in a lower effective mode index (see Fig. 2 where m for different Rs is given). However, for TM polarization, the n_{eff} is further smaller compared to the TE case (because of smaller m for TM). As a result, a smaller n_{eff} increases the leakage and coupling of the TM mode to the radiation modes.

#130161 - $15.00 USD Received 14 Jun 2010; revised 18 Aug 2010; accepted 24 Aug 2010; published 30 Aug 2010

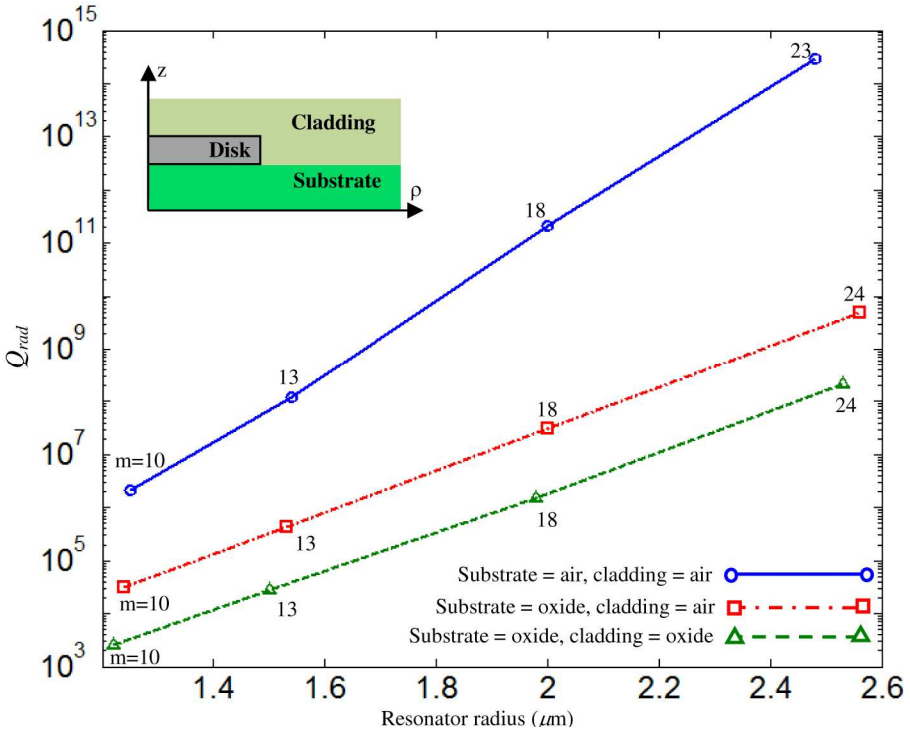

Fig. 2. Variation of the radiation Q of the 1st radial order TE mode of a miniaturized silicon microdisk resonator with a thickness of 230 nm versus its radius for three different cases as shown in the legend of the figure. The markers correspond to the obtained simulation points. The azimuthal harmonic mode number (m) of each resonance mode is shown next to each mode number. In all the simulations the radius of the microdisk is adjusted such that the resonance wavelength is in the range 1550 ± 10 nm. The refractive indices of silicon, oxide and air are assumed to be 3.475, 1.444, and 1, respectively. The inset shows the cross section of the microdisk in the cylindrical coordinate.

We initially consider a miniaturized Si microdisk and study the effect of its radius, the substrate, and the cladding on the radiation Q of the resonator. Figure 2 shows the calculated radiation Q of the first radial order TE mode of this resonator at different small radii for the following cases: 1- both substrate and cladding are SiO_2; 2- substrate is SiO_2 and the cladding is air; and 3- both substrate and cladding are air. Figure 2 clearly shows the large impact of the index contrast between the resonator and the surrounding material on the Q_{rad} of the resonator, especially at smaller radii where bending loss is higher. When both substrate and cladding are oxide (which is the most practical case) and the disk radius is ~1.2 μm, the Q_{rad} is on the order of ~2600. For such a case, if the fabrication condition is good, then the Q_i can be dominantly defined by the Q_{rad} and not limited by scattering Q (Q_{scat}) [17].

As discussed in section 1, a microdisk can be multimode in the radial direction which may not be desirable for some applications. However, when moving to smaller radii (e.g., r < 2.5 μm), higher radial order modes become very radiative. This is because they have a smaller effective index which becomes much lower than the first radial order mode at smaller radii. Hence, the bending loss for higher order modes is expected to be much larger. To design a single mode miniaturized resonator, it is enough to concentrate on the first and the second radial order modes and try to make the Q_{rad} of the second order mode as low as possible while preserving the Q_{rad} of the first order mode at a high level. By doing so, the Q_{rad} of other radial order modes (with radial mode orders more than 2) becomes automatically very small or negligible. The strategies pursued to achieve the single mode operation over a wide wavelength range (or the entire *FSR*) can be summarized as follows:

#130161 - $15.00 USD Received 14 Jun 2010; revised 18 Aug 2010; accepted 24 Aug 2010; published 30 Aug 2010

1. Higher radial order modes can be pushed to the strongly radiative region by changing the disk structure to a donut (i.e., a thick ring) shape as discussed before. By doing this modification, the effective index of the first radial mode is less affected while those of higher order modes (which have more interaction with the internal wall of the resonator) are reduced, especially, when the radial order becomes larger. In addition, because of the roughness induced at sidewalls by fabrication imperfections, the higher order modes suffer from Rayleigh scattering from the two sidewalls while the first radial order modes is exposed only to the outer sidewall.

2. The dimensions of the resonator can be adjusted in such a way that the resonance frequency of the 1st order radial mode is as far as possible from those of the higher order modes. As a result, the resonator can operate in the single mode condition for a large wavelength range.

3. The excitation of a resonator is normally through an adjacent waveguide. Therefore, if the waveguide-resonator coupling for higher order modes is weak, they do not contribute to the transmission spectrum. The strength of waveguide-resonator coupling is strongly dependent on the phase matching between the waveguide mode and the resonator mode, and the waveguide-resonator spacing. By proper engineering of the waveguide-resonator coupling geometry, we can considerably reduce the waveguide-resonator coupling strength for higher order modes of the resonator [23] and suppress them from the transmission spectrum (i.e., we avoid coupling to higher order modes to essentially achieve single mode resonance operation).

4. Lowering the thickness of the resonator can strongly reduce the mode effective index, especially for higher order modes. Correspondingly, their Q_{rad} can strongly reduce.

In this paper, we only pursue the first two methods mentioned above for the single mode resonator design (for example for the third method, Ref [23]. can be seen for more details of waveguide-resonator coupling).

In a microdisk, when the radius becomes smaller, the first radial order is more localized and concentrated toward the edge of the disk. This fact has been shown in Fig. 3 by comparing the energy distribution of the first radial order mode of the disk with respect to the disk edge for different radii. Hence, as mentioned earlier, by knowing the radial distribution of the first radial order mode we can appropriately perforate an inner hole into the center of the disk to form a donut for minimal (maximal) interaction with first (higher) order mode (modes). For more clarification, Fig. 4 shows the simulation results for the first and the second radial order modes of a microdonut resonator with an external small radius of 2.05 μm and with various internal radii, with both substrate and cladding being oxide. The external radius is selected to have all the resonances of the 1st and 2nd radial order mode close to each other (around ~1550 nm) to have a fair comparison of their Q_{rad}. As we see from Figs. 4(a)–4(d), we can reduce the donut width down to a point where the first radial order has negligible interaction with the inner wall of the donut, while the 2nd radial mode is subject to strong interaction with the two sidewalls of the donut. Figures 4(e) and 4(f) show the Q_{rad} and the resonance wavelengths of the 1st and the 2nd radial order modes for different donut widths, respectively. As seen from these figures, by reducing the donut width (W), the Q_{rad} and the resonance wavelength of the first order mode have very small changes. This is an evidence of the weak interaction of the internal wall of the donut. One can take the benefit of the weak interaction of the resonance mode profile of the microdonut with the internal microdonut wall to have a fine resonance wavelength control (i.e. sub-nanometer) for the 1st order mode by applying a relatively large change to the internal radius [see Fig. 4(f), the red plot]. This is especially advantageous when we have resolution limitation in lithography where we want to

#130161 - $15.00 USD Received 14 Jun 2010; revised 18 Aug 2010; accepted 24 Aug 2010; published 30 Aug 2010

fabricate resonators with resonance frequencies very close to each other. The second radial mode, however, is dramatically affected by reducing the donut width. This can be seen from Fig. 4(e) and 4(f) through the large changes in Q and the resonance wavelength, respectively. As an example from the table, for the donut width of W = 700 nm, the 1st radial order mode has its Q_{rad} almost intact, while that of 2nd order mode has reduced down below 300. By appropriate waveguide-resonator coupling design [23], the contribution of the 2nd order mode to the transmission spectrum can be suppressed.

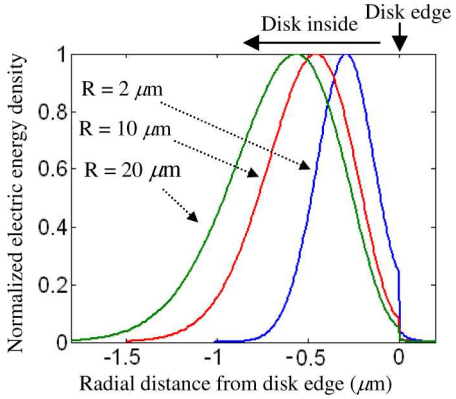

Fig. 3. Radial distribution of the normalized-to-peak electric energy density of the 1st order radial TE mode for Si microdisk resonators with a thickness of 230 nm and different radii R = 2 μm, 10 μm, and 20 μm, as specified in the figure. The point 0 in the horizontal axis corresponds to the position of the outside edge of the microdisk. All plots are for the variations of energy across a line in the radial direction and passing through the middle of the microdisk thickness.

When replacing a microring by a microdisk or a microdonut resonator to achieve a higher Q_i, another important physical parameter of resonator which needs to be considered is the electromagnetic mode volume (V_m) defined as

$$V_m = \frac{\int n^2 \mid E \mid^2 dv}{(\mid nE \mid_{\max})^2} \tag{6}$$

where $|E|$ represents the electric field magnitude; n is the refractive index; and the integration is performed over the entire space to consider the mode distribution. Knowing that the enhancement and sensitivity of light-matter interaction is proportional to Q/V_m, it is important to know how the mode volume changes when replacing the ring by a disk or donut. In a TWR, the radial and vertical confinements of the mode energy, as well as the resonator traveling length (which is proportional to the radius), determine the energy localization and mode volume of the resonator. While the vertical confinement for both the microring and the microdisk resonator architecture on the same substrate is almost the same, the microring has stronger radial confinement enforced by two sidewalls of the microring. However, as seen in Fig. 3, when shrinking the radius of a microdisk, the mode is highly localized at the edge of the disk. Therefore, we intuitively expect the radial mode confinement of the disk to approach the same level as that of a microring with a given typical width (e.g., 500 nm). To verify this, we calculated the mode volumes of both microring and microdisk resonator architectures for different diameters.

#130161 - $15.00 USD Received 14 Jun 2010; revised 18 Aug 2010; accepted 24 Aug 2010; published 30 Aug 2010

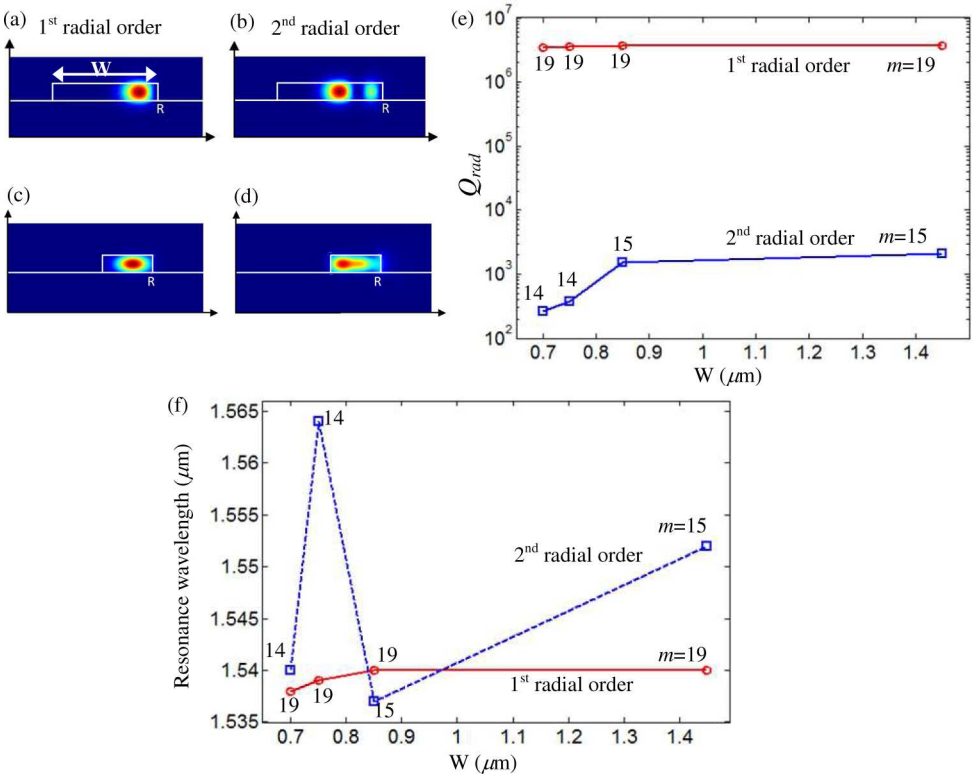

Fig. 4. (a)-(d) The cross sections of the mode energy of the 1st and the 2nd radial mode order of a microdonut resonator with an external radius of 2.05 μm, and widths (W)s of 1.45 μm and 0.85 μm, respectively. The silicon layer has a thickness of 230 nm and is surrounded by an oxide cladding. (e) and (f) Variation of the radiation Q and the resonance wavelength of the microdonut for the first 2 radial order modes for a fixed external radius of 2.05 μm versus different donut widths. The azimuthal mode number m (shown for each simulation point) is chosen in such a way that the resonance wavelength to be in the range of 1550 ± 15 nm.

Figure 5 shows the variation of the mode volume of the 1st, 2nd, and 3rd order radial TE modes of a Si microdisk as well as that of the fundamental TE mode of a Si microring resonator (with a width of 500 nm) versus their external diameters. All these resonators have a thickness of 230 nm and are on a SiO_2 substrate and covered by air. As seen from Fig. 5, for a microdisk, the mode volume of the 1st order radial mode is the smallest compared to its higher-order radial modes. For the same external diameter, the mode volume of a microring is smaller than that of all the modes of the microdisk. At smaller resonator diameters, the mode volumes of the modes of the microdisk and microring approach each other. This is especially clear for the 1st TE modes of the microdisk and microring. This can be simply explained through what we observe in Fig. 3, where at smaller radii, the radial confinement of the mode energy is smaller and more localized toward the edge of the microdisk. In other words, in a microdisk, when going to smaller radii (i.e., ~1.5 μm), the effective radial width of the mode energy becomes smaller and is comparable and almost at the same level as that of a microring with the same radius and a width > 500 nm. Hence, at smaller disk radii, we take one further action by modifying the disk to a donut in which the 1st radial mode is strongly confined and higher-order radial modes can be pushed to cut-off.

#130161 - $15.00 USD Received 14 Jun 2010; revised 18 Aug 2010; accepted 24 Aug 2010; published 30 Aug 2010

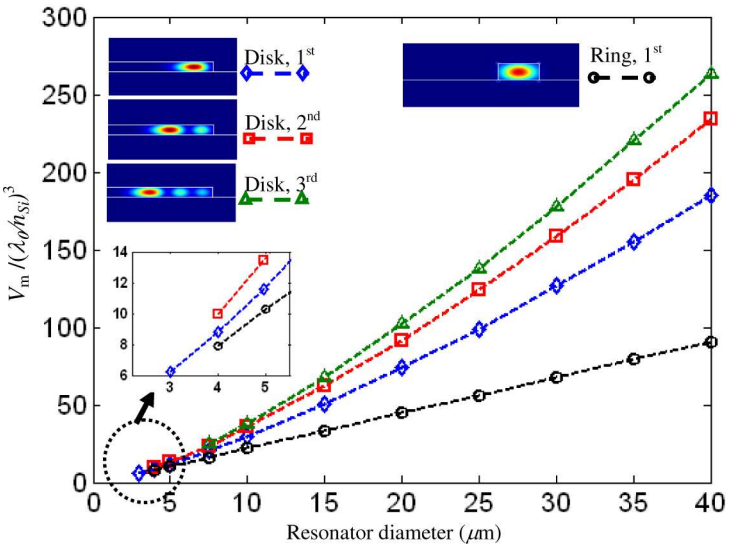

Fig. 5. Calculated normalized mode volume ($V_m /(\lambda_0/n_{Si})^3$) of the first three radial TE modes of a Si microdisk resonator, as well as the one for the fundamental TE mode of a microring resonator versus their outer diameters. In all the resonators, the resonator thickness is 230 nm, the substrate is SiO_2, and the cladding is air. The microring width is 500 nm. For all the simulations, the mode volume was calculated for one of the resonance wavelengths (λ_0) that existed in the range of 1550 ± 20 nm.

2.2 Miniaturized resonators compatible with active integration

As previously demonstrated [3], by adding a thin Si slab at the interface of a microring resonator and the underlying substrate, the resonator can be integrated with a p-n junction. Correspondingly, high-speed modulators and switches can be realized. A smaller resonator can reduce the power consumption of such modulators. At smaller resonator radii, a simultaneous presence of oxide cladding and the Si slab layer (which are essential in the integration of p-n junction) can dramatically increase the energy leakage of the resonator mode. The slab thickness has to be large enough to ensure efficient electron transport from the p-n junction and through the slab layer. In a recent report, a 30 nm slab thickness in a Mach-Zehnder interferometer is shown to be sufficient for high-speed electron transport [24] from the p-n junction to the arm of the Mach-Zehnder device. In this section, we have analyzed the Q_{rad} of a microdonut resonator with different slab thicknesses and donut widths. The intention to employ the microdonut architecture is to preserve a high Q for the 1st radial order mode and potentially suppress higher-order modes. Figures 6(a) and 6(b) show the cross section of the mode profiles of the 1st and the 2nd radial order TE modes of such a resonator with an external radius of 2.5 μm, a donut width of 1 μm, and a thin Si slab thickness of P = 50 nm. Both substrate and the cladding are oxide. From these two figures we see that 2nd radial order mode has more leakage to the outside as well as more interaction with the internal sidewalls of the donut compared to the 1st radial order mode. To have a quantitative comparison between these two modes, we have calculated their Q_{rad}. Figure 6(c) shows the Q_{rad} of a 1st and the 2nd radial order modes of the microdonut resonator versus its external radius at different thin Si slab thicknesses (P) and donut widths (W). From this analysis, we see that the Q_{rad} of the 2nd radial order mode is dramatically reduced while a high Q_{rad} for the 1st radial order mode is still achievable. For instance, at a radius of 2.5 μm, with a thin Si slab thickness of P = 30 nm and a donut width of 800 nm, the 2nd order mode has Q_{rad} ~130, while the Q_{rad} of the 1st radial mode for the same resonator is ~2.8×10^6 which is very high. The results shown in Fig. 6 suggest that the advantages of a microdonut resonator are not affected by the addition of the thin Si slab layer. Thus, microdonut resonators can be integrated with p-n

#130161 - $15.00 USD Received 14 Jun 2010; revised 18 Aug 2010; accepted 24 Aug 2010; published 30 Aug 2010

junction in a way similar to microring resonators without losing high Q, small mode volume, single mode operation, and compact size.

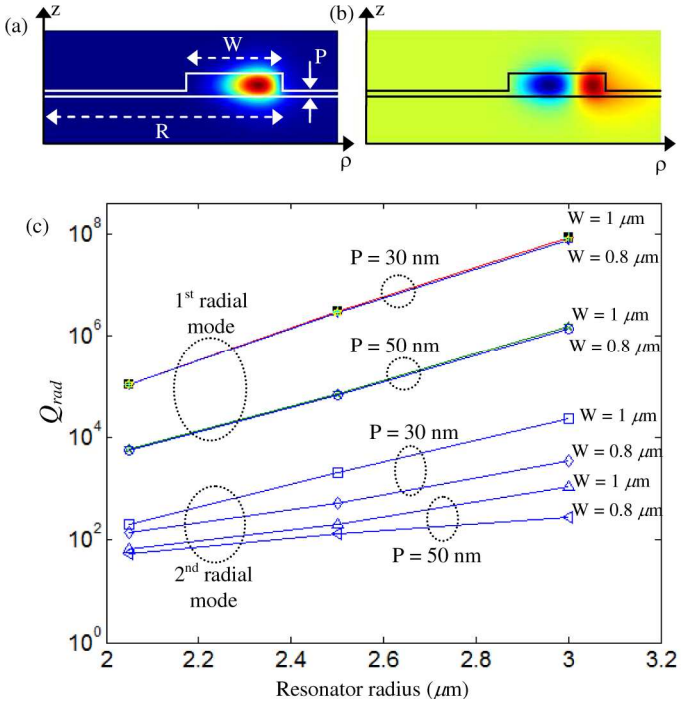

Fig. 6. Cross section of the z component of the magnetic field profile (H_z) of (a) the 1st and (b) the 2nd radial order modes of a microdonut resonator with a radius of R = 2.5 μm and a width of W = 1 μm, seated on a thin silicon slab layer with a thickness of P = 50 nm. (c) Calculated Q of the 1st and the 2nd radial order TE modes of a Si microdonut resonator versus its external radius for different donut widths and thin slab thicknesses as specified in the figure. In all simulations, both the substrate and the cladding are oxide, the silicon thickness is 230 nm, and the calculated Q is for one of the resonance wavelengths (λ_0) that exists in the range of 1550 ± 25 nm.

3. Fabrication and characterization of miniaturized resonators

We fabricate miniaturized resonators with radii ranging from 1.5 μm to 2.5 μm to experimentally study their performance. The resonators are fabricated on an SOI wafer with Si thicknesses ranging from 210 nm to 230 nm seated on top of a 1 μm thick buried oxide substrate. The devices are patterned using a JEOL JBX-9300FS electron beam lithography (EBL) system. The electron resist used is HSQ (which is a negative resist) with a thickness of 110 nm. After the lithography, the patterns are etched in chlorine-based plasma in an inductively-coupled plasma reactive ion etching system. At the end of etching, the remaining HSQ (with an approximate thickness of 60 nm) is kept. For the cases that the cladding is oxide, a 2 μm thick oxide is deposited on the sample using a plasma-enhanced chemical vapor deposition (PECVD). The details of the optical characterization setup can be found in [16].

#130161 - $15.00 USD Received 14 Jun 2010; revised 18 Aug 2010; accepted 24 Aug 2010; published 30 Aug 2010

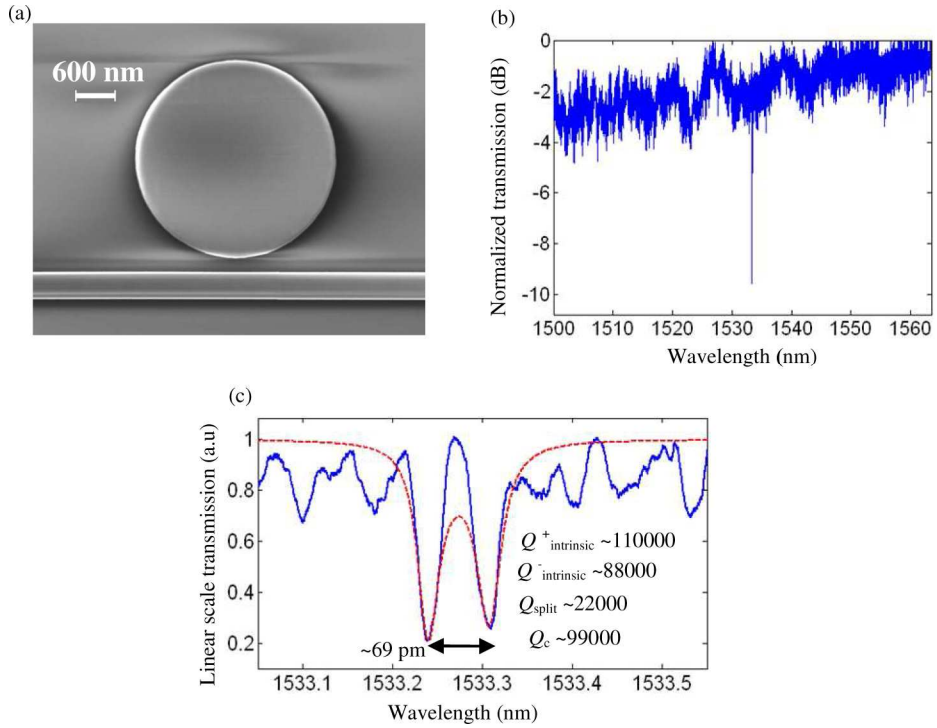

Fig. 7. (a) SEM image of a microdisk resonator with a radius of ~1.53 μm coupled to a waveguide with a width of 400 nm. The gap between the waveguide and the resonator is ~210 nm. The thickness of the Si microdisk is 213 nm, and there is a thin HSQ layer with a thickness of ~60 nm on top of the microdisk and the waveguide. (b) Transmission spectrum of the resonator showing the 1st radial order TE mode. (c) Detailed resonance spectrum of the 1st radial order TE mode of the resonator in (a), which shows resonance splitting. By fitting theory to experiment, the intrinsic Q's ≈110,000 and 88,000 are obtained for the two standing-wave modes. The value of the coupling Q (Q_c) is ~99,000 in the fitted data is close to the calculated value from coupled-mode theory. The azimuth harmonic mode number of this mode is m = 13 and its mode volume is ~6.3 $(\lambda_0/n)^3$ with n = 3.475.

Figure 7(a) shows the scanning electron microscopy (SEM) image of a microdisk resonator with a radius of 1.53 μm coupled to a straight ridge waveguide with a width of 400 nm. The substrate is oxide and the cladding is air. Figure 7(b) shows the transmission spectrum of this resonator for which only one resonance mode with strong extinction is seen over the entire *FSR* range. This resonance mode is the 1st radial order TE mode, and the theoretical simulations accurately predict it with an azimuth mode number m = 13. From the simulations, the *FSR* and the mode volume of this mode are *FSR* ≈70 *nm* and $V_m = 6.3\ (\lambda_0/n)^3$ (with n = 3.475), respectively. Figure 7(c) shows a zoomed view of the resonance mode spectrum shown in Fig. 7(b). As seen from Fig. 7(c), resonance splitting due to the coupling between the degenerate clockwise (CW) and counterclockwise (CCW) modes (because of fabrication-induced surface roughness) results in two standing-wave modes. A quality factor of Q_{split} is designated to this resonance splitting, and it is calculated as [17,21]

$$Q_{split} = \frac{4}{|\int \delta\varepsilon\, E_{CW}^{*} E_{CCW}\, dv|} = \frac{\lambda_0}{\Delta\lambda_{split}} \tag{7}$$

where $\delta\varepsilon$ is the permittivity perturbation of the resonator, λ_0 is the resonance wavelength, $\Delta\lambda_{split}$ is the wavelength split, and E_{cw} and E_{ccw} are respectively, the electric fields of the CW and CCW modes of the resonator normalized to their mode energy. By fitting the

#130161 - $15.00 USD Received 14 Jun 2010; revised 18 Aug 2010; accepted 24 Aug 2010; published 30 Aug 2010

experimental data into the theoretical simulations using the coupled mode theory of waveguide-resonator coupling (including the mutual coupling of CW and CCW modes of the resonator) [21,25], the resonator Q's can be obtained. From the fitting results, the intrinsic Q's of ~110,000 and 88,000 are obtained for the two standing-wave modes of this resonator (with conservative consideration of the Fabry-Perot distortion). Theoretical simulation shows that a resonator with such dimensions has the Q_{rad} ~4.5×10^5 while experiment shows total intrinsic Q_i in the order of 10^5. This shows that the achieved Q_i is still limited by scattering and fabrication imperfections. Also, the appearance of the resonance splitting is further evidence that the resonator Q_i is dominated by fabrication-induced scattering. By further optimizing the fabrication process, the Q has the potential to be improved at least four folds to reach what is shown in Fig. 2 (i.e., 4.5×10^5).

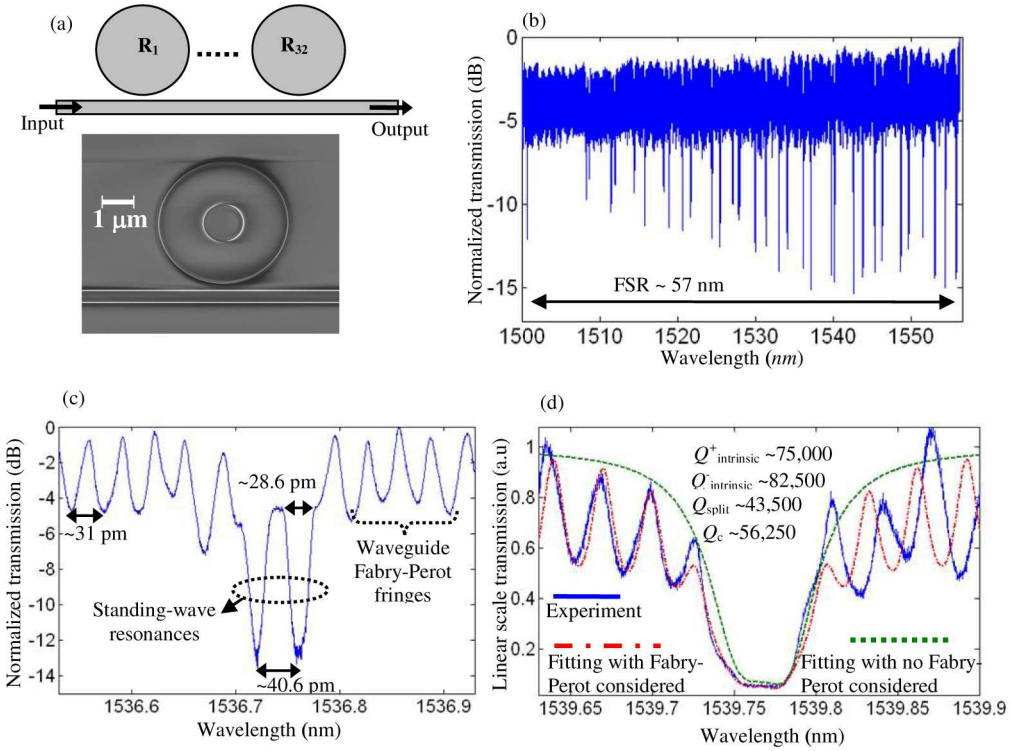

Fig. 8. (a) Top: An array of 32 donut resonators side coupled to a waveguide. Bottom: The SEM image of one of the resonators in the array. The structure has oxide cladding. An inner hole with a radius of 0.6 μm has been made at each disk center. The external radius of the resonators in the array is distributed in the range of 1.92 μm to 2 μm. (b) The resonance spectrum of the resonators array shown in (a). (c) and (d) The details of two of the resonance features shown in (b). These resonances belong to two different resonators with 5 nm difference in their external radii. In (c), resonance splitting with a doublet in the transmission is observed. In (d) resonance splitting has resulted in the flattening of the transmission. Strong Fabry-Perot fringes of the waveguide with a period of ~31 pm are observed. By fitting theory and experiment in (d) intrinsic Q's of ~82,500 and 75,000 are obtained for the two standing-wave modes of the resonator.

For a small microdisk with a radius ~1.5 μm, adding an oxide cladding significantly reduces the Q_{rad} as theoretically shown in Fig. 2. Hence, to preserve a high Q_{rad} while adding an oxide cladding, we increase the radius to ~2 μm. To better study this resonator (i.e., its high Q properties, single mode operation, fabrication induced randomness), we make an array of these resonators with slightly different radii from each other (near ~2 μm) coupled to a straight waveguide, as shown in Fig. 8(a). The array includes 32 individual resonators with

#130161 - $15.00 USD Received 14 Jun 2010; revised 18 Aug 2010; accepted 24 Aug 2010; published 30 Aug 2010

radii distributed in the range of 1.92 μm to 2 μm so that their resonance wavelengths are distributed in almost the entire FSR (which is ~57 nm from theoretical calculations). The SEM picture in Fig. 8(a) shows one of these resonators in the array before adding the oxide cladding. An inner hole with a radius of 0.6 μm has been perforated at the center of each disk to form a donut resonator. A 2 μm oxide deposited by plasma-enhanced chemical vapor deposition (PECVD) used as cladding on top of the resonators. Figure 8(b) shows the transmission response of the 32 resonators in the array shown in Fig. 8(a). As seen from Fig. 8(b), strong power extinctions for all the resonators are observed. Figures 8(c) and 8(d) show a detailed view of the resonance spectra of two microdonuts with a 5 nm difference in their radius. As seen from Fig. 8(c), resonance splitting with the appearance of a doublet with a wavelength splitting of 40.6 pm is observed. In general, when a doublet is observed, the coupling Q (Q_c) is larger than the splitting Q (Q_{split}) [21 (see chapter 3)]. By reducing the Q_c of the waveguide resonator toward and below the Q_{split}, the doublet in the resonance spectrum moves toward flattening and becoming a singlet. Figure 8(d) shows a scenario in which a very weak doublet is observed in the spectrum, and the transmission response around the center resonance is almost flattened. Although, the Q_c for the resonators of Figs. 8(c) and 8(d) are almost the same, the randomness in the fabrication has resulted in different sidewall roughness and consequently different Q_{split}. By fitting the experimental data to the theory, we are able to extract the Q_i of ~75,000 and 82,500 for the standing wave modes in Fig. 8(d). It is noted that because the period of Fabry-Perot fringes (from the facets of the chip) is comparable to the linewidth of the resonance, the Fabry-Perot effect can strongly load the resonator and make the resonator spectrum broader. Therefore, in the fitting, the effect of the Fabry-Perot fringes has to be considered. The red dashed-dotted curve in Fig. 8(d) shows the result of the fitting when the Fabry-Perot effect is considered and the green dotted curve is when the Fabry-Perot is absent. In other words, when Fabry-Perot fringes from the facets of the chip exists in the experiment; the measured linewidth of the experimental resonance spectrum is larger than the actual linewidth of the resonator.

In the experiment in Fig. 8, by scanning the wavelength of laser source over the FSR range and imaging of the resonators by a CCD camera it is observed that each resonator gets bright only at one wavelength which corresponds to its resonance. In addition, this imaging verifies that each resonator in the array is single mode. This is in agreement with what discussed in theory section, where for such small resonators with an oxide cladding, the 2nd and higher-order modes were predicted to be strongly leaky, and as a result, they have a very weak coupling to the waveguide. However, to gather further experimental evidence of this, another structure is designed and fabricated, as shown in the inset of Fig. 9. This structure is a 1st order add-drop filter made of a single resonator. The resonator and the waveguide dimensions and their spacing are similar to those of the resonator array in Fig. 8. Figure 9 shows the transmission spectrum of the drop port of this add-drop filter. As seen from Fig. 9, two resonance modes are observed, which are the 1st radial order TE modes with a wavelength FSR ~57 nm and azimuth mode numbers m = 18 and m = 19, corresponding to the longer and the shorter resonance wavelengths, respectively. The resonance wavelength locations and the FSR of these modes agreed well with the theoretical simulations. From the measurements, a linewidth of ~50 pm is measured for the resonances of this filter. As seen from Fig. 9, only the 1st radial order mode appears in the power transmission spectrum, and other higher radial order modes are below the noise floor. From the temporal coupled-mode theory [26], the normalized power transmission of the drop port in Fig. 9 and at resonance is

$$T(\omega_0) = \frac{1}{(1+0.5Q_c / Q_i)^2} \tag{8}$$

where, as mentioned, Q_i is the intrinsic Q of the resonator mode, and Q_c is the coupling Q of the resonator mode to one of the waveguides (we have assumed that Q_c of both waveguides to

#130161 - $15.00 USD Received 14 Jun 2010; revised 18 Aug 2010; accepted 24 Aug 2010; published 30 Aug 2010

the resonator in Fig. 9 is the same). Using Eq. (8) and from the spectrum in Fig. 9 we can say that Q_c for higher radial order modes is much higher than their Q_i which has resulted in the weak transmission (below noise floor in Fig. 9) for these modes. Knowing that such a large contrast exists between the Q_c and Q_i for the higher radial order modes, we can make some conclusions on the behavior of the higher order modes of the resonators in Fig. 8(which have similar waveguide-resonator dimensions with the one in Fig. 9 (i.e. nearly similar Q_c and similar Q_i)). In addition, the resonator modes in Fig. 8 need the critical coupling condition (i.e. $Q_c \sim Q_i$) to show strong transmission in the spectrum. However, as mentioned before, for the higher order modes Q_c is much larger that Q_i, which confirms their absence in the transmission spectrum in Fig. 8(b).

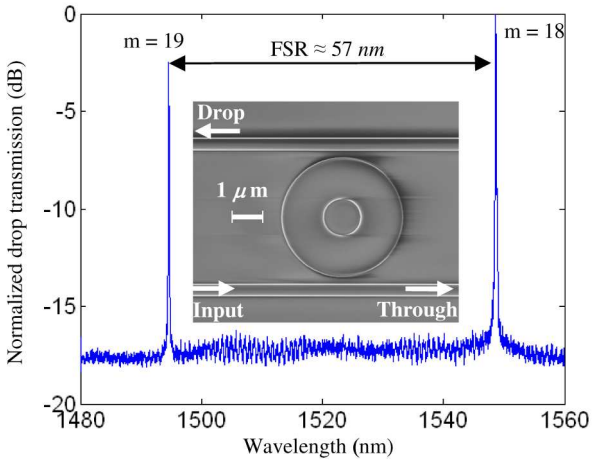

Fig. 9. The SEM image of a miniaturized add-drop filter before covering with oxide. The waveguide width and thickness are 400 *nm* and 230 *nm*, respectively. The employed microdisk resonator has a radius of r = 1.97 μm with an inner hole with a radius of r = 0.6 μm at its center. The gap between the waveguide and the resonator is 240 *nm*. The final structure has an oxide cladding. (b) Transmission spectrum of the drop port of the filter showing the two resonances belonging to the 1st order radial family modes with azimuth mode numbers (m) specified in the figure.

We also fabricate miniaturized resonators compatible with active integration. In our design, we consider a target thin Si slab [P in Fig. 6(a)] of 35 nm. For a microdonut with an external radius of 2 μm, a thin slab thickness of 35 nm, and an oxide cladding, we observe a very low Q_i and leaky resonator, confirming our theoretical calculations in Fig. 6. Therefore, we increased the resonator radius to reduce the radiative leakage and as a result increase the Q_i. Considering these facts, a microdonut resonator with an external radius of 2.5 μm, an internal radius of 1.3 μm, on a thin Si slab layer is fabricated. The measured thickness of the slab layer (after fabrication) using the ellipsometry technique is 33 nm, while the Si device layer is 216 nm. Figure 10(a) shows the transmission spectrum of this resonator coupled to a waveguide. The inset in Fig. 10(a) shows the SEM image of this resonator coupled to a waveguide with a width of 400 nm. The gap between the waveguide and the resonator is 250 nm. The structure is covered by a 2 μm layer of PECVD oxide, which is close to a realistic case where the resonator is integrated with a p-n junction. As can be seen from Fig. 10(a), three resonances belonging to the 1st radial order TE mode and with different azimuth mode numbers are observed. Figure 10(b) shows a zoomed view of one of the resonances in Fig. 10(a) with an azimuth mode number m = 23. A measured loaded spectral linewidth of ~115 pm is obtained for this resonance mode with an extinction of ~15 dB as shown in Fig. 10(b). Correspondingly, the Q_i of this resonator is ~24,000 which is very far from that of the ideal resonator (Q_{rad} >10^6) due to the fabrication imperfections. The presence of the thin

#130161 - $15.00 USD Received 14 Jun 2010; revised 18 Aug 2010; accepted 24 Aug 2010; published 30 Aug 2010

slab layer increases the chance of coupling of the microdisk mode to the leaky radiation modes in the slab due to surface roughness. We also note that by reducing the slab thickness to zero we expect the Q_i to increase as observed in our experimental results (see Fig. 8). While this Q_i is not large, this resonator can still be employed for many applications where this level of Q is satisfactory. As an example, a 2nd order coupled-resonator filter (with a bandwidth of ~1 nm at 1550 nm) made of two resonators with the mentioned Q_i has an insertion loss less than 1 dB. However, by improving the fabrication process, the Q_i of this architecture with such small radii can be further improved.

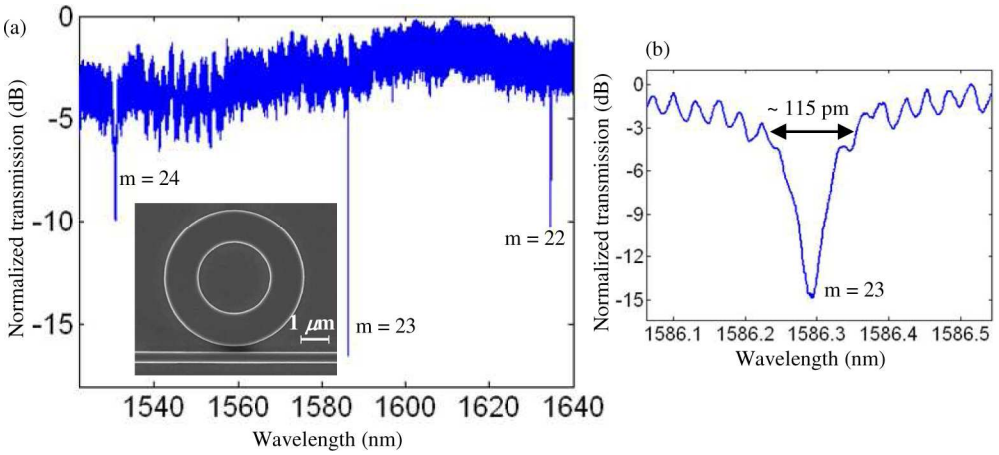

Fig. 10. (a) Transmission spectrum of a Si microdonut resonator seated on a thin Si slab. Inset shows the SEM image of the resonator. The resonator has internal and external radii of 1.3 μm and 2.5 μm, respectively, and coupled to a waveguide with a width of 400 nm. The gap between the waveguide and the resonator is 250 nm. The thickness of the underneath thin slab layer is 33 nm and the overall height of the Si device layer is 216 nm. (b) A zoomed view of one of the resonance modes.

In this paper our emphasis is to preserve the high Q_i properties of the resonator while shrinking its size. When the fabrication quality is good and the resonator becomes further smaller, the Q_i of the resonator is ultimately dominated by the Q_{rad} of the resonator. This is true, especially with the recent progresses in nanofabrication of Si photonic structures that have dramatically reduced the roughness of the sidewalls of the fabricated waveguides and resonators. As an example, for a microdisk with a radius ~1.22 μm with both substrate and cover being oxide, the Q_{rad} from Fig. 2 is ~2,600. Hence, with the current available good fabrication technology, we expect to get such a Q for the resonator. In such an operation regime, phenomena like resonance splitting (which is a signature of the fabrication limited regime) never occur. However, lack of resonance splitting does not mean that the resonator is in the radiation limit. A low waveguide-resonator coupling lifetime (i.e., a strong waveguide-resonator coupling) or low resonator scattering lifetime compared to the CW-CCW coupling lifetime (which is normally high) can result in a singlet response instead of a splitting response in the spectrum of the resonator.

In addition to the mentioned advantages of microdisk and microdonuts over a microring, a microdisk is very promising for applications where the high-speed and efficient thermal tuning of the resonator is needed. In microdisk architectures, a heater electrode can be directly seated on the Si microdisk (which is highly thermally conductive) [27]. The heater electrode is deposited close to the center of the disk and far from the perimeter of the disk [27]. In this manner, while thermal energy is efficiently delivered to the resonator, the 1st radial order mode of the microdisk (which is close to the perimeter) is not perturbed and higher order modes are further suppressed by the presence of the metallic heater electrode.

#130161 - $15.00 USD Received 14 Jun 2010; revised 18 Aug 2010; accepted 24 Aug 2010; published 30 Aug 2010

4. Conclusion

In this paper, we presented Si microdisk and microdonut resonators as promising elements for miniaturized photonic functionalities in an SOI platform. We showed that miniaturized microdisks and microdonuts have several advantages over the conventionally used microrings without sacrificing any performance measures. We showed that at very small radii, all the higher radial order modes of microdisk becomes strongly radiative and can leave the microdisk as a single mode resonator over the entire *FSR*. In addition, the mode volume of the miniaturized microdisk is similar to that of a microring with the same radius, while a much higher intrinsic Q can be obtained for a microdisk. To further guarantee the single mode condition, by adding a hole at the center of the disk and forming a donut (which is a thick ring), higher order modes are subject to stronger leakage while the first radial mode is almost intact. As the resonator is traveling-wave architecture, its excitation through a waveguide is very dependent on the phase matching between the waveguide and the resonator mode. Because different radial modes of a microdisk have different effective indices, their coupling to a waveguide are different. Therefore, a proper waveguide-resonator coupling design can add another degree of freedom to suppress all the higher order modes from the transmission spectrum. We demonstrated single mode Si resonators with radii as small as 1.5 μm, *FSR*~70 nm and $Q_i > 10^5$ when substrate is oxide and cladding is air. To preserve a high Q_i for the resonator with both substrate and cladding being oxide, we increased the radius to ~2 μm and demonstrated a single mode resonator with Q_i ~80,000 and *FSR* ~57 nm. We believe such miniaturized microdisks and microdonuts can replace conventionally used microrings in Si photonic structures to enable much denser integration of optical functionalities, much larger operation bandwidth and much faster, low-power reconfiguration compared to existing devices.

Acknowledgments

This work was supported by Air Force Office of Scientific Research under Contract No. FA9550-06-01-2003 (G. Pomrenke). The authors would like to thank Farshid Ghasemi for the useful discussions and comments on this paper.

#130161 - $15.00 USD Received 14 Jun 2010; revised 18 Aug 2010; accepted 24 Aug 2010; published 30 Aug 2010